Global Exponential Tracking Control for an Autonomous Surface Vessel: An Integral Concurrent Learning Approach

Zachary Ian Bell, Jason Nezvadovitz, Anup Parikh, Eric M. Schwartz, *Senior Member, IEEE*, and Warren E. Dixon, *Fellow, IEEE*

***Abstract*—In this paper, an adaptive controller is developed for a fully actuated marine vehicle where the rigid body and hydrodynamic parameters are unknown. A data-based integral concurrent learning method is used to compensate for the uncertain parameters. A Lyapunov-based analysis is presented to show that the closed-loop system is globally exponentially stable and the uncertain parameters are identified exponentially without the requirement of persistence of excitation. Experimental results on an autonomous surface vessel operating on a lake illustrate the controller's ability to track figure-8 trajectories in environments with small disturbances.**

***Index Terms*—Adaptive control, integral concurrent learning (ICL), marine craft, nonlinear control, parameter identification, uncertain dynamics.**

I. Introduction

CONTROLLING marine craft, such as autonomous underwater vehicles (AUVs) and surface vessels (ASVs), is motivated by potential efficiencies related to shipping commerce, law enforcement, and national security efforts. Accurate control is required to maintain optimal path following, navigating in congested and narrow harbors, docking, etc. However, a challenge for accurate positioning is uncertainty in the dynamics of the vessel. For example, one source of uncertainty in the rigid body parameters of a marine craft is due to the addition of shipping containers, which change the mass, moment of inertia, and center of gravity. Additionally, uncertain hydrodynamic effects that are difficult to approximate lead to an effective added mass, Coriolis-centripetal forces, and viscous damping [1]. Such uncertain effects motivate the development of control techniques that can provide robustness to parametric uncertainties.

Manuscript received August 11, 2017; revised March 16, 2018 and August 21, 2018; accepted October 30, 2018. Date of publication December 12, 2018; date of current version April 14, 2020. This work was supported in part by the NEEC under Grant/Award N00174-18-1-0003, in part by AFOSR under Grant/Award FA9550-18-1-0109, in part by the Office of Naval Research under Grant/Award N00014-13-1-0151, and in part by NSF under Grant/Award 1509516 and under Grant/Award 1762829. *(Corresponding author: Zachary Ian Bell.)*

Associate Editor: B. Bingham.

Z. I. Bell, J. Nezvadovitz, A. Parikh, and W. E. Dixon are with the Department of Mechanical and Aerospace Engineering, University of Florida, Gainesville, FL 32611-6250 USA (e-mail: bellz121@ufl.edu; jnezvadovitz@ufl.edu; anuppari@ufl.edu; wdixon@ufl.edu).

E. M. Schwartz is with the Department of Electrical and Computer Engineering, University of Florida, Gainesville, FL 32611-6250 USA (e-mail: ems@ufl.edu).

Digital Object Identifier 10.1109/JOE.2018.2880622

Robust control strategies, such as [2] and [3], exploit the use of high (infinite) frequency or high gains to dominate worst case uncertainty that is typically modeled as an additive disturbance. For example, a sliding mode controller is developed in [2] to enable an ASV, modeled by nonlinear Euler–Lagrange dynamics, to track a desired trajectory. A high gain feedback, input–output linearization-based, robust steering autopilot is developed in [3] that yields local stability through a pole placement strategy, where a high gain observer is used to provide robustness without an accurate plant model nor any information about the uncertainties and disturbances. The robust integral sign of the error (RISE)-based control strategy (e.g., [4] and [5]) exploits both high gain and high frequency to yield global asymptotic tracking for uncertain ASVs and AUVs, in [6] and [7], respectively.

Motivated to reduce the high gain and/or high frequency feedback components developed for the worst case uncertainty, various results augment controllers with adaptive feedforward terms. For example, results in [8]–[16] develop controllers that use neural networks (NNs) or fuzzy logic to approximate the uncertain dynamics up to some residual error. Specifically, such results combine a model-free feedforward function approximation term with robust feedback to yield uniform ultimately bounded results, where the residual error stems from the approximation error and disturbances. The result in [7] combines an NN with RISE feedback to eliminate the residual error and achieve semiglobal asymptotic tracking for an AUV.

ASV dynamics have been extensively modeled with uncertainties that satisfy the linear in the unknown parameters assumption (cf., [17] and [18]). Hence, in contrast to the aforementioned NN or fuzzy-logic-based model-free function approximation methods, results such as [17] and [19]–[21] exploit structural knowledge of the dynamics to achieve asymptotic results using model-based adaptive controllers. Unless a persistence of excitation (PE) condition is satisfied, such controllers generally yield asymptotic (versus exponential) tracking results without any guarantees of parameter identification (cf., [7], [17], [19], and [20]) and can exhibit the bursting phenomenon [22]. However, for nonlinear systems it is not possible, in general, to verify if the PE condition is satisfied, even if ad hoc perturbations are injected to excite the system.

The results in [23]–[27] provide an online model approximation method called concurrent learning that can be used in

lieu of the PE assumption with a milder finite excitation condition that can be verified online. Concurrent learning updates estimates of the unknown parameters based on input and output data of the dynamic system. However, such methods require the derivative of the highest order state (often computed numerically), and then use various filtering methods to reduce the noise from the higher order terms. In this paper and the preliminary result in [28], an *integral* concurrent learning (ICL) method is developed, which reformulates the traditional concurrent learning problem to remove the need for the derivative of the highest order state and related filtering. Specifically, a globally exponentially stable tracking controller is developed using ICL for a fully actuated ASV with uncertain rigid body and hydrodynamic parameters. In comparison to the precursory result in [28], the development in this paper includes an expanded model development section, provides experimental results that demonstrate the performance and implementation issues with the developed controller, and provides an expanded summary and conclusion. Before sufficient excitation is obtained, a Lyapunov-based analysis is used to prove the error trajectories globally converge to a residual error, where the residual is a function of the parametric uncertainty. Once sufficient (finite) excitation is satisfied, further analysis is used to conclude global exponential tracking and parameter identification; hence, the potential bursting phenomena is also eliminated. To illustrate the performance of developed controller, experimental results are provided for a fully actuated ASV equipped with a Sylphase GPS/INS system operating on a lake. The experimental results indicate that the developed controller yields ultimately bounded errors near the GPS/INS accuracy while demonstrating robustness to small unmodeled external disturbances, e.g., choppy water, light wind, and sensor noise. Additionally, the experimental results indicate that as the dynamic model is learned, the control effort almost entirely shifts from high frequency content feedback terms to feedforward terms with lower frequency content.

II. Dynamic Model

In the following development, the body fixed frame and the world fixed frame are defined as shown in Fig. 1. The body fixed origin and the body center of gravity are assumed to lie along the centerline of the ASV. The gravitational forces are assumed to balance with the buoyancy forces acting on the body, and wave and wind forces are neglected. Given these assumptions, the dynamics of the ASV can be expressed in the body fixed frame similar to [18, Ch. 7.1, 7.1.2, and 13.3.7] as

$$M\dot{\nu} + C(\nu)\nu + D(\nu)\nu = \tau$$

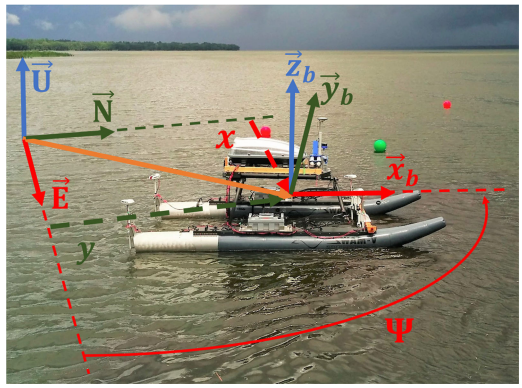

Fig. 1. University of Florida NaviGator ASV experimental testbed. The body fixed frame of the ASV has the directions $\{\vec{x}_b, \vec{y}_b, \vec{z}_b\}$ and origin on the centerline. The world fixed frame (i.e., the East, North, up frame) has the directions $\{\vec{E}, \vec{N}, \vec{U}\}$ and origin determined as the initial location of the ASV. The position of the ASV in the world fixed frame is given by the states $x(t)$ and $y(t)$ and the orientation given by the state $\Psi(t)$. The length of the overall vessel is approximately 4.9 m, the distance from the aft to the center of gravity is approximately 1.4 m, the beam of the individual pontoons is approximately 0.8 m, the draft is approximately 0.2 m, and the mass is approximately 500 kg.

where $\nu(t) \triangleq [\, u \;\; v \;\; r_\Psi \,]$, where $u, v \in \mathbb{R}$ denote the linear body velocities along $\vec{x}_b$ and $\vec{y}_b$ and $r_\Psi \in \mathbb{R}$ is the yaw rate expressed in the body fixed frame; $\dot{\nu}(t)$ is the acceleration expressed in the body fixed frame; and

$$M \triangleq \begin{bmatrix} m - X_{\dot{u}} & 0 & 0 \\ 0 & m - Y_{\dot{v}} & mx_g - Y_{\dot{r}} \\ 0 & mx_g - Y_{\dot{r}} & I_z - N_{\dot{r}} \end{bmatrix}$$

where $m, x_g, X_{\dot{u}}, Y_{\dot{v}}, Y_{\dot{r}}, I_z, N_{\dot{r}} \in \mathbb{R}$ are the unknown constant rigid body and hydrodynamic inertia terms. In addition, we have the first equation shown at the bottom of the page, which is the rigid body and hydrodynamic matrix of Coriolis and centripetal terms, and the second equation shown at the bottom of this page, where $X_{|u|u}, Y_{|v|v}, Y_{|r|v}, Y_{|v|r}, Y_{|r|r}, N_{|v|v}, N_{|r|v}, N_{|v|r}, N_{|r|r} \in \mathbb{R}$ are the unknown constant hydrodynamic maneuvering terms. $\tau(t) \in \mathbb{R}^3$ is the control input. The dynamics can be expressed in the world fixed frame as discussed in [18, Ch. 7.1 and 13.3.7] as

$$M^*(\Psi)\ddot{\eta} + C^*(\nu, \Psi)\dot{\eta} + D^*(\nu, \Psi)\dot{\eta} = R(\Psi)\tau \qquad (1)$$

by exploiting the fact that the body velocity can be expressed in the world fixed frame through the relationship $\dot{\eta} = R(\Psi)\nu$, where $\Psi(t) \in \mathbb{R}$ is the orientation (yaw) of the body fixed frame with respect to the world fixed frame;

$$C(\nu) \triangleq \begin{bmatrix} 0 & 0 & -mx_g r_\Psi - mv + Y_{\dot{v}} v + Y_{\dot{r}} r_\Psi \\ 0 & 0 & mu - X_{\dot{u}} u \\ mx_g r_\Psi + mv - Y_{\dot{v}} v - Y_{\dot{r}} r_\Psi & -mu + X_{\dot{u}} u & 0 \end{bmatrix}$$

$$D(\nu) \triangleq \begin{bmatrix} -X_{|u|u}|u| & 0 & 0 \\ 0 & -Y_{|v|v}|v| - Y_{|r|v}|r_\Psi| & -Y_{|v|r}|v| - Y_{|r|r}|r_\Psi| \\ 0 & -N_{|v|v}|v| - N_{|r|v}|r_\Psi| & -N_{|v|r}|v| - N_{|r|r}|r_\Psi| \end{bmatrix}$$

$R(\Psi) \in \mathbb{R}^{3\times 3}$ is the rotation matrix of the body fixed frame with respect to the world fixed frame; $\eta(t) \triangleq [x\ y\ \Psi]^T$, where $x, y \in \mathbb{R}$ is Cartesian position of the ASV in the world fixed frame; $\dot{\eta}(t), \ddot{\eta}(t)$ denote velocity and acceleration vectors expressed in the world fixed frame, respectively; $M^*(\Psi) \triangleq R(\Psi) M R^T(\Psi)$; $C^*(\nu, \Psi) \triangleq R(\Psi)(C(\nu) - M R^T(\Psi)\dot{R}(\Psi))R^T(\Psi)$; and $D^*(\nu, \Psi) \triangleq R(\Psi) D(\nu) R^T(\Psi)$.

Property 1: The inertia matrix is positive definite and symmetric as shown in [18, Ch. 13.3.7], and may be bounded as follows:

$$m_1\|\zeta\|^2 \leq \zeta^T M^*(\Psi)\zeta \leq m_2\|\zeta\|^2 \ \ \forall \zeta \in \mathbb{R}^3$$

where $m_1, m_2 \in \mathbb{R}$ are positive scalar constants and $\|\cdot\|$ is the Euclidean norm.

The time derivative of the inertia matrix is skew symmetric with the matrix of Coriolis and centripetal terms [18, Ch. 13.3.7] as

$$\zeta^T \left(\frac{1}{2}\dot{M}^*(\Psi) - C^*(\nu, \Psi)\right)\zeta = 0 \quad \forall \zeta \in \mathbb{R}^3.$$

The Euler Lagrange dynamics in (1) are linear in the unknown constant parameters and can be represented as [17]

$$Y_1(\nu, \Psi, \dot{\eta}, \ddot{\eta})\theta = M^*(\Psi)\ddot{\eta} + C^*(\nu, \Psi)\dot{\eta} + D^*(\nu, \Psi)\dot{\eta} \tag{2}$$

where $Y_1(\nu, \Psi, \dot{\eta}, \ddot{\eta}) \in \mathbb{R}^{3\times p}$, and $\theta \in \mathbb{R}^p$ represents the unknown constant parameters.

III. Control Design

A. Tracking Error Development

To quantify the control objective, let $e(t) \in \mathbb{R}^3$ and $r(t) \in \mathbb{R}^3$ denote a tracking error and an auxiliary tracking error, respectively, defined as follows:

$$e \triangleq \eta_d - \eta \tag{3}$$

$$r \triangleq \dot{e} + \alpha e \tag{4}$$

where $\eta_d(t) \in \mathbb{R}^3$ represents the continuous desired body position and yaw trajectory in the world fixed frame with known continuous first and second time derivatives $\dot{\eta}_d(t), \ddot{\eta}_d(t) \in \mathbb{R}^3$, and $\alpha \in \mathbb{R}^{3\times 3}$ is a constant, positive definite, and diagonal gain matrix. To facilitate the analysis, the first time derivative of the auxiliary tracking error in (4) is premultipled by $M^*(\Psi)$ to yield

$$M^*(\Psi)\dot{r} = M^*(\Psi)(\ddot{\eta}_d + \alpha\dot{e}) - M^*(\Psi)\ddot{\eta}.$$

Using (1) and performing some algebraic manipulation yields

$$M^*(\Psi)\dot{r} = Y_2(\nu, \Psi, \eta, \dot{\eta}, \eta_d, \dot{\eta}_d, \ddot{\eta}_d)\theta - R(\Psi)\tau - C^*(\nu, \Psi)r \tag{5}$$

where the measurable (i.e., numerically known) matrix $Y_2(\nu, \Psi, \eta, \dot{\eta}, \eta_d, \dot{\eta}_d, \ddot{\eta}_d) \in \mathbb{R}^{3\times p}$ can be combined with the uncertain parameters defined in (2) as

$$Y_2\theta = M^*(\Psi)(\ddot{\eta}_d + \alpha\dot{e}) + C^*(\nu, \Psi)(\dot{\eta}_d + \alpha e) + D^*(\nu, \Psi)\dot{\eta}. \tag{6}$$

B. Parameter Identification Error System Development

To facilitate learning the constant rigid body parameters and hydrodynamic effects online, a parameter identification error, $\tilde{\theta}(t) \in \mathbb{R}^p$, is defined as follows:

$$\tilde{\theta} \triangleq \theta - \hat{\theta} \tag{7}$$

where $\hat{\theta}(t) \in \mathbb{R}^p$ is the unknown parameter estimate. Based on the subsequent stability analysis, the parameter estimate update law is designed as

$$\dot{\hat{\theta}} \triangleq \Gamma Y_2^T r + \Gamma k_2 \sum_{i=1}^{N} \mathcal{Y}_i^T \left(\mathcal{U}_i - \mathcal{Y}_i\hat{\theta}\right) \tag{8}$$

where $\Gamma, k_2 \in \mathbb{R}^{p\times p}$ are constant, positive definite, and diagonal gain matrices, $N \in \mathbb{Z}$ is a positive, constant integer representing the size of the concurrent learning history stack, $t_i \in [\Delta t, t]$ are time points between the initial time and the current time, $\Delta t \in \mathbb{R}$ is a positive design constant denoting the size of the window of integration, $\mathcal{Y}_i \triangleq \mathcal{Y}(t_i)$ and $\mathcal{U}_i \triangleq \mathcal{U}(t_i)$ are defined as follows:

$$\mathcal{Y}(t) \triangleq \begin{cases} 0_{3\times p}, & t \in [0, \Delta t] \\ \int_{t-\Delta t}^{t} Y_1(\nu(\sigma), \Psi(\sigma), \dot{\eta}(\sigma), \ddot{\eta}(\sigma))\, d\sigma, & t > \Delta t \end{cases} \tag{9}$$

$$\mathcal{U}(t) \triangleq \begin{cases} 0_{3\times 1}, & t \in [0, \Delta t] \\ \int_{t-\Delta t}^{t} R(\Psi(\sigma))\tau(\sigma)\, d\sigma, & t > \Delta t \end{cases} \tag{10}$$

and $0_{3\times p}$ denotes a $3 \times p$ matrix of zeros. The summation term in (8) represents a history stack of input and output data generated by the dynamics. Substituting $Y_1\theta$ for the left-hand side of (1) using the definition in (2), integrating both sides, and using the definitions in (9) and (10) yields

$$\mathcal{Y}\theta = \mathcal{U} \quad \forall t > \Delta t. \tag{11}$$

The integral formulation in (9) and (10) removes the dependence on higher order derivatives. Specifically, integrating both sides of (2) yields

$$\begin{aligned} \int_{t-\Delta t}^{t} Y_1(\nu(\sigma), \Psi(\sigma), \dot{\eta}(\sigma), \ddot{\eta}(\sigma))\theta d\sigma &= \int_{t-\Delta t}^{t} M^*(\Psi(\sigma))\ddot{\eta}(\sigma)\, d\sigma \\ &+ \int_{t-\Delta t}^{t} C^*(\nu(\sigma), \Psi(\sigma))\dot{\eta}(\sigma)\, d\sigma \\ &+ \int_{t-\Delta t}^{t} D^*(\nu(\sigma), \Psi(\sigma))\dot{\eta}(\sigma)\, d\sigma \end{aligned} \tag{12}$$

$\forall t > \Delta t$. The dependence on the acceleration is removed by integrating $M^*(\Psi)\ddot{\eta}$ by parts as

$$\begin{aligned} \int_{t-\Delta t}^{t} M^*(\Psi(\sigma))\ddot{\eta}(\sigma)\, d\sigma = \ & M^*(\Psi(t))\dot{\eta}(t) \\ & - M^*(\Psi(t-\Delta t))\dot{\eta}(t-\Delta t) \\ & - \int_{t-\Delta t}^{t} \dot{M}^*(\Psi(\sigma))\dot{\eta}(\sigma)\, d\sigma \end{aligned}$$

and then substituting into (12) to yield

$$\int_{t-\Delta t}^{t} Y_1\left(\nu\left(\sigma\right),\Psi\left(\sigma\right),\dot{\eta}\left(\sigma\right),\ddot{\eta}\left(\sigma\right)\right)\theta d\sigma = Y_3\left(\Psi,\dot{\eta}\right)\theta + \int_{t-\Delta t}^{t} Y_4\left(\nu\left(\sigma\right),\Psi\left(\sigma\right),\dot{\eta}\left(\sigma\right)\right)\theta d\sigma \tag{13}$$

where the regression matrices $Y_3\left(\Psi,\dot{\eta}\right), Y_4\left(\nu,\Psi,\dot{\eta}\right) \in \mathbb{R}^{3\times p}$ are defined as follows:

$$Y_3\left(\Psi,\dot{\eta}\right)\theta \triangleq M^*\left(\Psi\left(t\right)\right)\dot{\eta}\left(t\right) - M^*\left(\Psi\left(t-\Delta t\right)\right)\dot{\eta}\left(t-\Delta t\right) \tag{14}$$

$$Y_4\left(\nu,\Psi,\dot{\eta}\right)\theta \triangleq -\dot{M}^*\left(\Psi\right)\dot{\eta} + C^*\left(\nu,\Psi\right)\dot{\eta} + D^*\left(\nu,\Psi\right)\dot{\eta}. \tag{15}$$

The right-hand side of (13) can then be used to calculate $\mathcal{Y}$ without measuring $\ddot{\eta}$. Substituting (11) into (8), then applying the definition in (7), gives an equivalent nonimplementable form of the update law that is used in the subsequent analysis

$$\dot{\hat{\theta}} = \Gamma Y_2^T r + k_2 \Gamma \sum_{i=1}^{N} \mathcal{Y}_i{}^T \mathcal{Y}_i \tilde{\theta}. \tag{16}$$

C. Control Input Development

To achieve the control objective, the controller expressed in the body fixed frame is designed as

$$\tau \triangleq R\left(\Psi\right)^T\left(k_1 r + e + Y_2\hat{\theta}\right) \tag{17}$$

where $k_1 \in \mathbb{R}^{3\times 3}$ is a constant, positive definite, and diagonal gain matrix. Substituting (17) into (5) gives the closed-loop error dynamics

$$M^*\left(\Psi\right)\dot{r} = Y_2\tilde{\theta} - k_1 r - e - C^*\left(\nu,\Psi\right)r. \tag{18}$$

IV. Stability Analysis

From the design in (8), the PE criteria, traditionally required to prove parameter identification, is relaxed to a finite excitation condition given in Assumption 1.

Assumption 1: The system is sufficiently excited over a finite duration of time. Specifically, $\exists \lambda^* > 0$, $\exists T > \Delta t$ such that $\forall t \geq T, \lambda_{\min}\{\sum_{i=1}^{N} \mathcal{Y}_i^T \mathcal{Y}_i\} \geq \lambda^*$, where $\lambda_{\min}\{\cdot\}$ denotes the minimum eigenvalue of $\{\cdot\}$ (and $\lambda_{\max}\{\cdot\}$ denotes the maximum eigenvalue).[1]

Theorem 1: For the system defined in (1), the controller and adaptive update law defined in (17) and (8) ensure global bounded tracking and parameter estimation errors during the time interval $t \in [0, T]$.

Proof: Let $V\left(z\right): \mathbb{R}^{6+p} \to \mathbb{R}$ be a candidate Lyapunov function defined as follows:

$$V = \frac{1}{2}e^T e + \frac{1}{2}r^T M^*\left(\Psi\right)r + \frac{1}{2}\tilde{\theta}^T\Gamma^{-1}\tilde{\theta} \tag{19}$$

[1]See [29] for examples of methods to select data.

where $z \in \mathbb{R}^{6+p}$ be defined as $z \triangleq \left[\, e^T \;\; r^T \;\; \tilde{\theta}^T \,\right]^T$. Taking the first time derivative of (19), using (4), (7), (16), (18), and the fact that θ is constant yields

$$\dot{V} = e^T\left(r - \alpha e\right) + \frac{1}{2}r^T\dot{M}^*\left(\Psi\right)r + r^T\left(Y_2\tilde{\theta} - k_1 r - e - C^*\left(\nu,\Psi\right)r\right) - \tilde{\theta}^T\Gamma^{-1}\left(\Gamma {Y_2}^T r + \Gamma k_2 \sum_{i=1}^{N} {\mathcal{Y}_i}^T \mathcal{Y}_i \tilde{\theta}\right). \tag{20}$$

Since $\sum_{i=1}^{N} {\mathcal{Y}_i}^T \mathcal{Y}_i$ is positive semidefinite $\forall t < T$, using Property 1 and simplifying gives

$$\dot{V} \leq -e^T \alpha e - r^T k_1 r$$

implying the trajectories $e\left(t\right)$ and $r\left(t\right)$ remain bounded based on [30, Th. 8.4]. Furthermore, since $\dot{V} \leq 0, V\left(z\left(T\right)\right) \leq V\left(z\left(0\right)\right)$, and

$$\left\|z\left(T\right)\right\| \leq \sqrt{\frac{\beta_2}{\beta_1}}\left\|z\left(0\right)\right\|$$

where $\beta_1 \triangleq \left(1/2\right)\min\left\{1, m_1, \lambda_{\min}\{\Gamma^{-1}\}\right\}$ and $\beta_2 \triangleq \left(1/2\right)\max\{1, m_2, \lambda_{\max}\{\Gamma^{-1}\}\}$ using Property 1. ■

Theorem 2: For the system defined in (1), the controller and adaptive update law defined in (17) and (8) ensure global exponential tracking in the sense that

$$\left\|z\left(t\right)\right\| \leq \left(\frac{\beta_2}{\beta_1}\right)\exp\left(\lambda_1 T\right)\left\|z\left(0\right)\right\|\exp\left(-\lambda_1 t\right) \quad \forall t \in [0,\infty). \tag{21}$$

Proof: Using (19), (20), and Assumption 1, $\lambda_{\min}\{\sum_{i=1}^{N}\mathcal{Y}_i^T\mathcal{Y}_i\} > 0$, $\forall t \in [T,\infty)$, which implies that $\sum_{i=1}^{N}\mathcal{Y}_i^T\mathcal{Y}_i$ is positive definite $\forall t \in [T,\infty)$ and therefore $\dot{V}$ is upper bounded by a negative definite function of z during $t \in [T,\infty)$. Using Property 1, and simplifying gives

$$\dot{V} = -e^T\alpha e - r^T k_1 r - k_2 \sum_{i=1}^{N} {\mathcal{Y}_i}^T \mathcal{Y}_i \tilde{\theta} \quad \forall t \in [T,\infty). \tag{22}$$

Invoking [30, Th. 4.10], global exponential tracking is obtained in the sense that

$$\left\|z\left(t\right)\right\| \leq \sqrt{\frac{\beta_2}{\beta_1}}\left\|z\left(T\right)\right\|\exp\left(-\lambda_1\left(t-T\right)\right) \quad \forall t \in [T,\infty)$$

where $\lambda_1 \triangleq \left(1/\beta_2\right)\min\{\lambda_{\min}\{\alpha\}, \lambda_{\min}\{k_1\}, \lambda_{\min}\{k_2\}\lambda^*\}$. The composite vector can be further upper bounded using the results of Theorem 1, yielding (21). ■

V. Experiment

The University of Florida NaviGator ASV, shown in Figs. 1 and 2, was used to test the performance of the developed controller. The ASV consists of a WAM-V pontoon outfitted with electronics and thrusters. The vessel is 5 m long and 2.5 m wide and has a dry weight of roughly 340 kg. The two pontoons on the vessel are loosely coupled by the suspension and a single beam at the bow. As shown in Fig. 2, the vessel includes four

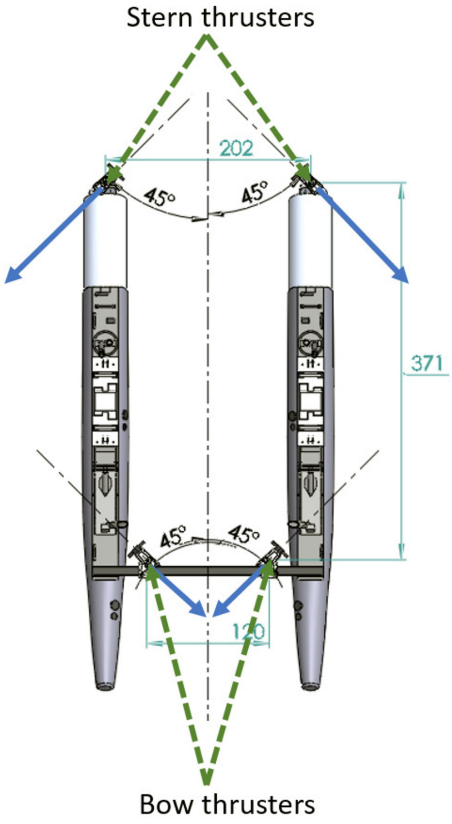

Fig. 2. Thruster configuration with units in centimeters and degrees. Each thruster remains fixed and blue arrows indicate positive thrust direction in body frame.

TABLE I
ROOT MEAN SQUARE OF THE TOTAL INPUT OVER EACH CYCLE

Total input	Cycle 1	Cycle 2	Cycle 3	Cycle 4
X-Force (N)	205.9	194.4	195.2	196.3
Y-Force (N)	34.6	28.2	28.0	29.2
Z-Moment (N·m)	140.6	130.5	128.3	129.3

TABLE II
ROOT MEAN SQUARE OF THE FEEDBACK INPUT OVER EACH CYCLE

Feedback input	Cycle 1	Cycle 2	Cycle 3	Cycle 4
X-Force (N)	105.5	29.9	27.5	25.6
Y-Force (N)	26.8	17.1	15.7	15.7
Z-Moment (N·m)	96.9	66.1	57.3	56.4

TABLE III
ROOT MEAN SQUARE OF THE FEEDFORWARD INPUT OVER EACH CYCLE

Feedforward input	Cycle 1	Cycle 2	Cycle 3	Cycle 4
X-Force (N)	185.3	210.1	207.2	202.1
Y-Force (N)	14.5	16.7	19.4	20.3
Z-Moment (N·m)	60.0	80.3	92.0	101.6

trolling motors to provide thrust, each fixed close to a corner of the vessel, i.e., two thrusters are mounted to the beam at the bow of the vessel and two thrusters are mounted at the stern of the vessel. As depicted in Fig. 2, the bow thrusters have positive thrust 45° inward, toward the centerline of the vessel, whereas the stern thrusters have positive thrust 45° outward, away from the centerline of the vessel. Each thruster is bidirectional and has a maximum thrust of approximately 220 N when traveling at the maximum velocity during steady-state. Specifically, the four thrusters yield maximum surge and sway speeds of approximately 1.3 and 0.5 m/s, respectively. Additionally, each thruster has a deadband of approximately 10 N (i.e., ± 5 N), where the deadband results because the propellers have no thrust when switching direction.

To implement the control input using the ASV thrusters, a box-constrained Tikhonov-regularized least-squares problem (cf., [31]) is solved where the box is defined by the maximum thrust possible by each thruster; however, during operation the developed controller gains are tuned such that the maximum thrust is never required and the least squares solution to the Tikhonov regularization is used. Given thrust mapping was not the focus of this result, the Tikhonov regularization was used because there are more thrusters than states and it yields an analytical solution. The controller development did not include actuator dynamics (i.e., the development assumes that the desired input can be instantly achieved); yet, the thrusters exhibit noticeable slew rates. Since the desired trajectory did not involve large accelerations, the slew rates had minimal impact on the results; however, for high performance during more aggressive maneuvers, additional development could focus on including such actuator effects in the control design. Such extensions can likely be achieved through the application of backstepping methods or a high gain feedback loop applied to the actuator dynamics. The vessel uses a Sylphase GPS/INS module attached to the electronics platform to provide full-state feedback. The module consists of a 3-axis accelerometer, 3-axis gyroscope, 3-axis magnetometer, barometer, and GPS receiver. State estimates are computed by the module using an extended Kalman filter which is updated at 100 Hz. Experimental testing of the sensing module indicated an initial positional accuracy of approximately 4 cm of root mean squared error, with an approximate drift of less than 60 cm after 1000 s, while orientation accuracy remained within fractions of a degree.

Experiments were performed on a lake when there was light rain and wind speeds of approximately 15 km/h from the North producing small waves approximately 5 cm tall and a slight current. These environmental conditions generated a small disturbing force and moment acting on the ASV not captured by the model in (1); however, experiments in these conditions showed that the developed adaptive estimator and controller demonstrated reasonable performance despite model inaccuracies and small disturbances.

Experiments were performed with a trajectory that has long strait line segments, which are not likely to be sufficiently exciting for the traditional PE condition. Specifically, the desired trajectory denoted by $\eta_d \triangleq [\, x_d \;\; y_d \;\; \Psi_d \,]^T$, where $x_d, y_d \in \mathbb{R}$ are the desired position and Ψ_d is the desired orientation in the inertial frame, is designed as a figure-8, which was computed parametrically using the lemniscate of Bernoulli equations as

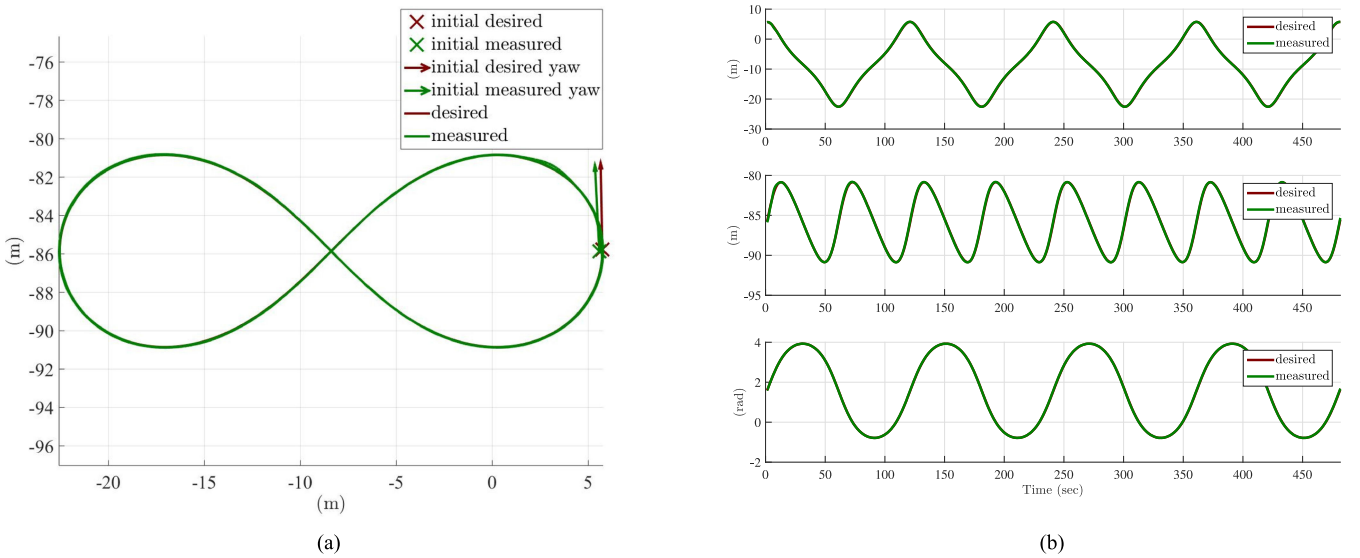

Fig. 3. Desired (red) and measured (green) position and orientation of the ASV. The Cartesian position is expressed in the world fixed frame and the orientation denotes the rotation of the body fixed frame with respect to the world fixed frame about the axis perpendicular to the plane (i.e., in Fig. 1). (a) Cartesian position of the ASV, where the vertical axis denotes the position along $\overrightarrow{N}$ world fixed axis, and the horizontal axis denotes the position along the $\overrightarrow{E}$ world fixed axis. (b) Desired and measured Cartesian position along the $\overrightarrow{E}$ world fixed axis (top), $\overrightarrow{N}$ world fixed axis (middle), and orientation of the body fixed frame with respect to the world fixed frame (bottom) versus time.

follows:

$$x_d = \frac{a\sqrt{2}\cos(\omega t)}{\sin^2(\omega t)+1}$$

$$y_d = \frac{a\sqrt{2}\cos(\omega t)\sin(\omega t)}{\sin^2(\omega t)+1}$$

where $a = 10$ m is the distance from the origin to a focal point, and $\omega = \pi/60$ rad/s is the cycle frequency. The desired orientation of the vessel was aligned with the tangent of the curve as

$$\Psi_d = \tan^{-1}\left(\frac{\dot{\eta}_{d_2}}{\dot{\eta}_{d_1}}\right).$$

These desired trajectories resulted in a figure-8 path. The ASV completed the figure-8 path in 120 s. The experiment included four cycles of the figure-8 path. The orientation of the ASV started approximately facing North into the wind.

The control and adaptation gains that yielded the results in Tables I–III and Figs. 3–7, are $k_1 = \text{diag}(1000,\ 1000,\ 6000)$, $\alpha = \text{diag}(0.9,\ 0.9, 0.93), \Gamma = 0.01\ I(13)$, and $k_2 = 200\ I(13)$, where $I(\cdot)$ is an identity matrix of size $(\cdot)$ and $\text{diag}(\cdot)$ is a diagonal matrix with the elements $(\cdot)$. The time window of integration used for concurrent learning was $\Delta t = 0.5$ s and $N = 100$ was used for the size of the history stack. All integrations were approximated numerically using the trapezoidal rule. The buffers used for integration and the history stack were treated as a first-in-first-out queue, with new data acquired at 100 Hz. The parameter estimate vector $\hat{\theta}$ was initialized with all zeros to indicate no knowledge of the uncertain parameters. In practice, the adaptive estimates would be initialized to the best guess estimates of the uncertain parameters.

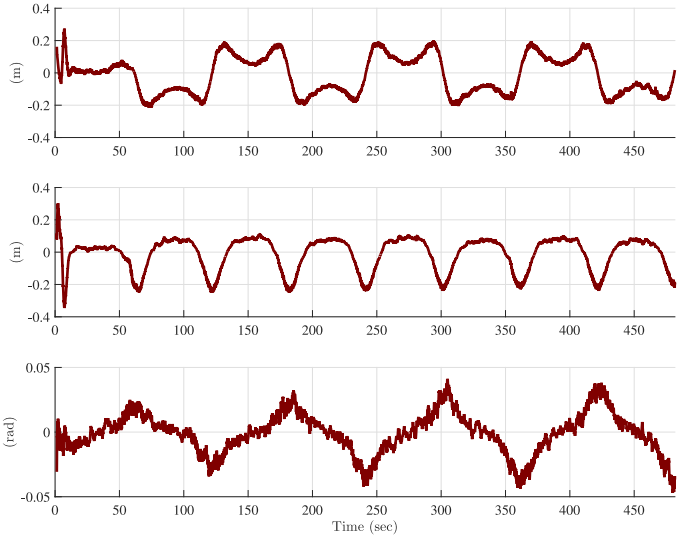

Fig. 4. Position tracking error along the $\overrightarrow{E}$ world fixed axis (top), $\overrightarrow{N}$ world fixed axis (middle), and orientation tracking error (bottom).

As shown in Figs. 3 and 4, the position and orientation tracking error remains low throughout the experiment. The root mean square of the error over the entire experiment was calculated to be approximately 12 cm for the error along the X-axis, 10 cm along the Y-axis, and 0.02 rad of yaw error. The root mean square of the auxiliary tracking error implies that the velocity tracking remained low with 12 cm/s along the X-axis, 10 cm/s along the Y-axis, and 0.02 rad/s of yaw rate error. These residual errors are the result of unmodeled disturbances, unmodeled actuator dynamics (e.g., slew rate of the thrusters), and measurement noise. Fig. 5 shows the evolution of the rigid body and hydrodynamic parameter estimates. While the true values

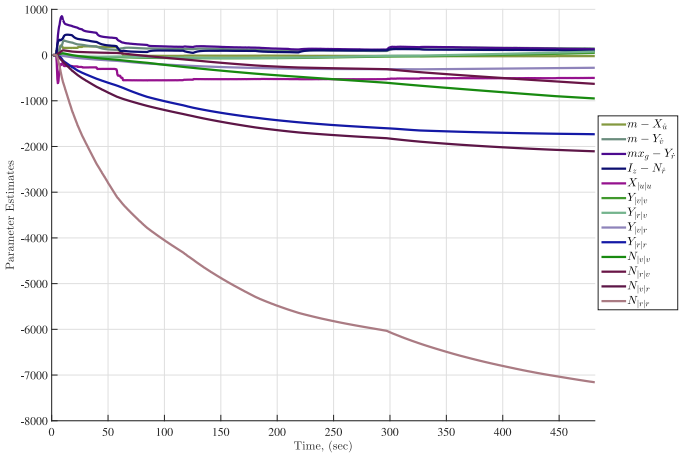

Fig. 5. Rigid body and hydrodynamic inertial parameter estimates.

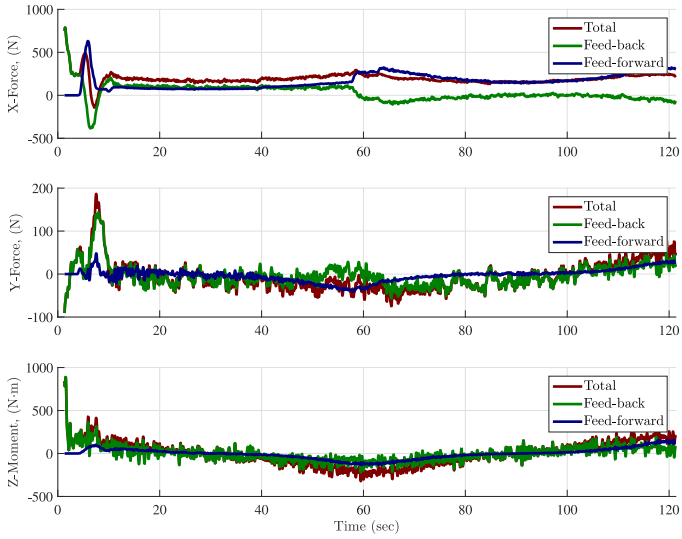

Fig. 6. Total (red) commanded input, feedback (green) components, and adaptive feedforward (blue) components for the first complete figure-8 trajectory. The top and middle plots indicate forces along the $\overrightarrow{E}$ and $\overrightarrow{N}$ world fixed axis, respectively, and the bottom plot indicates the moment about the $\overrightarrow{U}$ world fixed axis.

of the parameters are unknown, the parameter estimates are converging to values that qualitatively agree with Fossen's model. Additionally, it was noted that as the experiment progressed, the contribution by the feedback terms diminished and the adaptive feedforward term provided the primary contribution to the total control input. Specifically, Figs. 6 and 7 plot the total commanded input, $R(\Psi)^T\tau$, along with the contribution from the feedback terms, $R(\Psi)^T(k_1 r + e)$, and the feedforward terms, $R(\Psi)^T(Y_2\hat{\theta})$ during the first and fourth cycle of the figure-8 trajectory. Tables I–III provide the root mean square of the different control terms to illustrate how the required contribution by the feedback terms diminish, providing an indication of parameter learning. The feedback terms are primarily compensating for the unmodeled dynamics, such as slew rates of the thrusters, wind forces, and small waves, as well as noise in the measurements. To ensure robustness against such disturbances, the feedback terms require high gain amplification of the sensor measure-

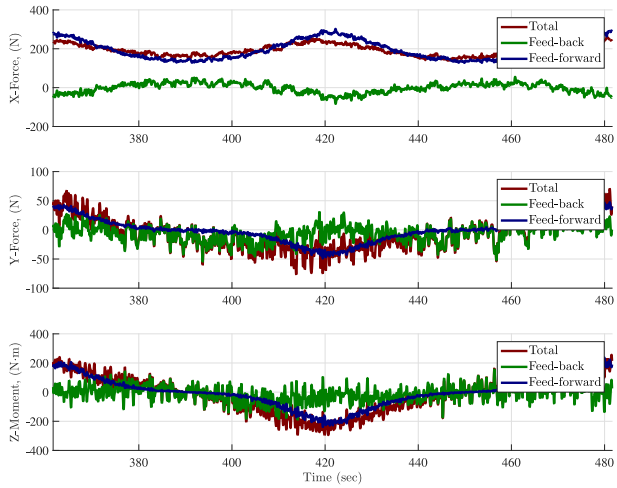

Fig. 7. Total (red) commanded input, feedback (green) components, and adaptive feedforward (blue) components for the fourth complete figure-8 trajectory. The top and middle plots indicate forces along the $\overrightarrow{E}$ and $\overrightarrow{N}$ world fixed axis, respectively, and the bottom plot indicates the moment about the $\overrightarrow{U}$ world fixed axis.

ments, in contrast to the feedforward component that provides robustness to the uncertainty through an adaptive approximation of the dynamics. The use of the ICL method facilitates learning the actual system parameters in comparison to traditional adaptive control methods that require persistent excitation. The experimental results illustrate that as more data are acquired, the ICL-based adaptive feedforward term contributes much more to the overall control effort than the feedback portion.

VI. Conclusion

The ICL based control scheme developed in this paper enables an ASV with unknown rigid body and hydrodynamic parameters to achieve global exponential tracking and parameter identification. The unique integral formulation of concurrent learning allowed for exponential convergence and parameter identification without requiring the PE condition to be satisfied and without higher order state derivatives (i.e., existing concurrent learning methods would require acceleration measurements along with filtering methods to compensate for high frequency content and traditional adaptive approaches require PE for parameter identification). Stability results were proven through a Lyapunov-based analysis and the performance of the controller was tested on an ASV operating on a lake with rain, light wind, and small waves. The experimental results demonstrated that the developed controller converged to an ultimate bound in practice given model uncertainties, wind and wave disturbances, and noise in state measurements; however, the RMS position and orientation errors were on the order of centimeters and fractions of a degree (near the limits of accuracy for the sensors) for a figure-8 trajectory with a path length covering tens of meters. Experimental results also indicate the equal or larger contribution by the feedback portion of the controller during transient periods with significantly higher contributions of the feedforward terms in comparison to feedback terms during the steady-state performance as evidence of the adaptation of the controller.

Future efforts could investigate the inclusion of actuator dynamics so that slew rate effects of the thrusters could be accounted for within the control design. Alternatively, the slew rate dynamics could potentially be modeled as a delayed response and results from input delay literature (cf., [32]–[34]) could be insightful. Experimental testing of the controller in a broader range of environmental conditions and comparing the results to results by other controllers may provide further insight into the robustness and performance of the developed controller.

In addition to the actuator dynamics, additional control efforts could be developed to account for the disturbances. For example, robust control strategies, such as sliding mode control or RISE control [7], could potentially be incorporated. Alternatively, incorporating ICL in function approximation methods, such as fuzzy logic or NNs, would be an interesting approach to compensate for a broader class of uncertainties.

ACKNOWLEDGMENT

Any opinions, findings, and conclusions or recommendations expressed in this material are those of the author(s) and do not necessarily reflect the views of the sponsoring agency.

REFERENCES

[1] T. I. Fossen, *Guidance and Control of Ocean Vehicles*. Hoboken, NJ, USA: Wiley, 1994.
[2] J. Cheng, J. Yi, and D. Zhao, "Design of a sliding mode controller for trajectory tracking problem of marine vessels," *IET Control Theory Appl.*, vol. 1, no. 1, pp. 233–237, Jan. 2007.
[3] S. Das and S. E. Talole, "Robust steering autopilot design for marine surface vessels," *IEEE J. Ocean. Eng.*, vol. 41, no. 4, pp. 913–922, Oct. 2016.
[4] P. M. Patre, W. MacKunis, K. Kaiser, and W. E. Dixon, "Asymptotic tracking for uncertain dynamic systems via a multilayer neural network feedforward and RISE feedback control structure," *IEEE Trans. Autom. Control*, vol. 53, no. 9, pp. 2180–2185, Nov. 2008.
[5] P. M. Patre, W. Mackunis, C. Makkar, and W. E. Dixon, "Asymptotic tracking for systems with structured and unstructured uncertainties," *IEEE Trans. Control Syst. Technol.*, vol. 16, no. 2, pp. 373–379, Mar. 2008.
[6] B. Bidikli, E. Tatlicioglu, and E. Zergeroglu, "A robust tracking controller for dynamically positioned surface vessels with added mass," in *Proc. 53rd IEEE Conf. Decis. Control*, 2014, pp. 4385–4390.
[7] N. Fischer, D. Hughes, P. Walters, E. Schwartz, and W. E. Dixon, "Nonlinear RISE-based control of an autonomous underwater vehicle," *IEEE Trans. Robot.*, vol. 30, no. 4, pp. 845–852, Aug. 2014.
[8] K. Venugopal, R. Sudhakar, and A. Pandya, "On-line learning control of autonomous underwater vehicles using feedforward neural networks," *IEEE J. Ocean. Eng.*, vol. 17, no. 4, pp. 308–319, Oct. 1992.
[9] J.-H. Li, P.-M. Lee, and Sang-Jeong-Lee, "Neural net based nonlinear adaptive control for autonomous underwater vehicles," in *Proc. IEEE Int. Conf. Robot. Autom.*, 2002, vol. 2, pp. 1075–1080.
[10] C. Wang and D. J. Hill, "Learning from neural control," *IEEE Trans. Neural Netw.*, vol. 17, no. 1, pp. 130–146, Jan. 2006.
[11] E. Sebastian and M. A. Sotelo, "Adaptive fuzzy sliding mode controller for the kinematic variables of an underwater vehicle," *J. Intell. Robot. Syst.*, vol. 49, no. 2, pp. 189–215, 2007.
[12] L.-J. Zhang, X. Qi, and Y.-J. Pang, "Adaptive output feedback control based on DRFNN for AUV," *Ocean. Eng.*, vol. 36, no. 9/10, pp. 716–722, 2009.
[13] L.-J. Zhang, H.-M. Jia, and X. Qi, "NNFFC-adaptive output feedback trajectory tracking control for a surface ship at high speed," *Ocean Eng.*, vol. 38, no. 13, pp. 1430–1438, 2011.
[14] S.-L. Dai, C. Wang, and F. Luo, "Identification and learning control of ocean surface ship using neural networks," *IEEE Trans. Ind. Inform.*, vol. 8, no. 4, pp. 801–810, Nov. 2012.
[15] B. S. Park, "Neural network-based tracking control of underactuated autonomous underwater vehicles with model uncertainties," *J. Dyn. Syst. Meas. Control*, vol. 137, no. 2, 2015, Art. no. 021004.
[16] B. S. Park, J.-W. Kwon, and H. Kim, "Neural network-based output feedback control for reference tracking of underactuated surface vessels," *Automatica*, vol. 77, pp. 353–359, 2017.
[17] Y. Fang, E. Zergeroglu, M. De Queiroz, and D. Dawson, "Global output feedback control of dynamically positioned surface vessels: an adaptive control approach," *Mechatronics*, vol. 14, no. 4, pp. 341–356, 2004.
[18] T. I. Fossen, *Handbook of Marine Craft Hydrodynamics and Motion Control*. Hoboken, NJ, USA: Wiley, 2011.
[19] R. Skjetne, Ø. N. Smogeli, and T. I. Fossen, "A nonlinear ship manoeuvering model: Identification and adaptive control with experiments for a model ship," *Model. Identification Control*, vol. 25, no. 1, pp. 3–27, 2004.
[20] R. Skjetne, T. I. Fossen, and P. V. Kokotović, "Adaptive maneuvering, with experiments, for a model ship in a marine control laboratory," *Automatica*, vol. 41, no. 2, pp. 289–298, 2005.
[21] W. B. Klinger, I. R. Bertaska, K. D. von Ellenrieder, and M. R. Dhanak, "Control of an unmanned surface vehicle with uncertain displacement and drag," *IEEE J. Ocean. Eng.*, vol. 42, no. 2, pp. 458–476, Apr. 2017.
[22] B. D. Anderson, "Adaptive systems, lack of persistency of excitation and bursting phenomena," *Automatica*, vol. 21, no. 3, pp. 247–258, 1985.
[23] G. V. Chowdhary and E. N. Johnson, "Theory and flight-test validation of a concurrent-learning adaptive controller," *J. Guid. Control Dyn.*, vol. 34, no. 2, pp. 592–607, Mar. 2011.
[24] G. Chowdhary, M. Mühlegg, J. How, and F. Holzapfel, "Concurrent learning adaptive model predictive control," in *Advances in Aerospace Guidance, Navigation and Control*, Q. Chu, B. Mulder, D. Choukroun, E.-J. van Kampen, C. de Visser, and G. Looye, Eds. Berlin, Germany: Springer, 2013, pp. 29–47.
[25] G. Chowdhary, T. Yucelen, M. Mühlegg, and E. N. Johnson, "Concurrent learning adaptive control of linear systems with exponentially convergent bounds," *Int. J. Adapt. Control Signal Process.*, vol. 27, no. 4, pp. 280–301, 2013.
[26] R. Kamalapurkar, J. Klotz, and W. E. Dixon, "Concurrent learning-based online approximate feedback Nash equilibrium solution of N-player nonzero-sum differential games," *IEEE/CAA J. Automatica Sinica*, vol. 1, no. 3, pp. 239–247, Jul. 2014.
[27] R. Kamalapurkar, B. Reish, G. Chowdhary, and W. E. Dixon, "Concurrent learning for parameter estimation using dynamic state-derivative estimators," *IEEE Trans. Autom. Control*, vol. 62, no. 7, pp. 3594–3601, Jul. 2017.
[28] Z. Bell, A. Parikh, J. Nezvadovitz, and W. E. Dixon, "Adaptive control of a surface marine craft with parameter identification using integral concurrent learning," in *Proc. IEEE Conf. Decis. Control*, 2016, pp. 389–394.
[29] G. Chowdhary and E. Johnson, "A singular value maximizing data recording algorithm for concurrent learning," in *Proc. Amer. Control Conf.*, 2011, pp. 3547–3552.
[30] H. K. Khalil, *Nonlinear Systems*, 3rd ed. Upper Saddle River, NJ, USA: Prentice-Hall, 2002.
[31] G. H. Golub, P. C. Hansen, and D. P. O'Leary, "Tikhonov regularization and total least squares," *SIAM J. Matrix Anal. Appl.*, vol. 21, pp. 185–194, 1999.
[32] I. Karafyllis, M. Malisoff, M. Queiroz, and M. Krstic, "Predictor-based tracking for neuromuscular electrical stimulation," *Int. J. Robust Nonlinear Control*, vol. 25, pp. 2391–2419, 2013.
[33] D. Bresch-Pietri and M. Krstic, "Delay-adaptive control for nonlinear systems," *IEEE Trans. Autom. Control*, vol. 59, no. 5, pp. 1203–1218, May 2014.
[34] S. Obuz, J. R. Klotz, R. Kamalapurkar, and W. E. Dixon, "Unknown time-varying input delay compensation for uncertain nonlinear systems," *Automatica*, vol. 76, pp. 222–229, Feb. 2017.

Zachary Ian Bell received the B.S. degree in mechanical engineering with a minor in electrical engineering in 2015 and the M.S. degree in mechanical engineering in 2017 from the University of Florida, Gainesville, FL, USA, where he is currently working toward the Ph.D. degree under the supervision of Dr. Warren E. Dixon in the nonlinear controls and robotics group.

His research interests include Lyapunov-based estimation and control theory, visual estimation, simultaneous localization and mapping, and mechanical design.

Mr. Bell was the recipient of the Science, Mathematics, and Research for Transformation (SMART) Scholarship, sponsored by the Department of Defense in 2018.

Jason Nezvadovitz received the B.S. degree in mechanical engineering with electrical engineering minor and the M.S. degree in dynamics and control theory, both with *summa cum laude*, from the University of Florida, Gainesville, FL, USA, in 2017.

As a student, he designed, manufactured, and programmed many robotic systems including a submarine, pontoon boat, and mobile 4-DOF manipulator. He is now a full-time Researcher with the Controls and Autonomy Group, MIT Lincoln Laboratory, Lexington, MA, USA, where he focuses on navigation and motion planning algorithms for high performance autonomous vehicles.

Anup Parikh received the B.S. degree in mechanical and aerospace engineering, the M.S. degree in mechanical engineering, and the Ph.D. degree in aerospace engineering from the University of Florida, Gainesville, FL, USA.

He is currently a Senior Member of the Technical Staff with the Robotics R&D Department, Sandia National Laboratories, Albuquerque, NM, USA. His primary research interests include Lyapunov-based estimation and control theory, machine vision, unmanned systems, and autonomous control.

Eric M. Schwartz (S'82–M'85–SM'02) received the B.S. degree in both electrical and mechanical engineering, the M.S. degree in electrical engineering, and the Ph.D. degree in electrical and computer engineering from the University of Florida, Gainesville, FL, USA, in 1984, 1989, and 1995, respectively.

During three semesters in 1980 and 1981, he worked with Bendix Avionics, Fort Lauderdale, FL, USA. In summer 1982, he worked with Universal Security Instruments, Baltimore, MD, USA. In summer 1983, he worked with International Business Machines, Boca Raton, FL, USA. In summer 1987, he worked with SASIAM and the Advanced Robotics Research Group of Technopolis, Bari, Italy. In summer 1988, he worked with Allen–Bradley Corporation, Cleveland, OH, USA. In 1989–1993, he worked with the Electronic Communications Laboratory, University of Florida. In 1985, he joined the Machine Intelligence Laboratory (MIL), University of Florida, as a Graduate Student Researcher, became a Postgraduate Researcher for MIL in 1995, the Assistant Director of MIL in 1998, the Associate Director in 2004, and the Director in 2016. In 1995–1997, he was a Visiting Assistant Professor in Electrical and Computer Engineering with the University of Florida, a Lecturer from 1997–2005, a Senior Lecturer from 2005–2008, and became a Master Lecturer in 2008.

Dr. Schwartz has been Treasurer or Secretary of the IEEE Gainesville Section since 2002 and the Faculty Advisor of the IEEE Gainesville Section Student Branch since 2002. He has directed many robot teams, including five world champions (three RoboSub, one RoboBoat, and one Maritime RobotX Challenge in 2016). His teams have competed in 14 out of the 25 world championships, in which they earned third or better. He was the recipient of the 2002–2003 University of Florida Teacher of the Year Award.

Warren E. Dixon (F'16) received the Ph.D. degree from the Department of Electrical and Computer Engineering, Clemson University, Clemson, SC, USA, in 2000.

He worked as a Research Staff Member and Eugene P. Wigner Fellow at Oak Ridge National Laboratory (ORNL) until 2004, when he joined the University of Florida with the Mechanical and Aerospace Engineering Department, where he currently serves as a Netwon C. Ebaugh Professor. His main research interest has been the development and application of Lyapunov-based control techniques for uncertain nonlinear systems.

Dr. Dixon is an ASME Fellow. He is currently or formerly an Associate Editor for the *ASME Journal of Dynamic Systems, Measurement and Control*, the *Automatica*, IEEE CONTROL SYSTEMS MAGAZINE, the IEEE TRANSACTIONS ON SYSTEMS MAN AND CYBERNETICS—PART B: CYBERNETICS, and the *International Journal of Robust and Nonlinear Control*. He was the recipient of the (2017–2018 and 2012–2013) University of Florida College of Engineering Doctoral Dissertation Mentoring Award, 2015, and 2009 American Automatic Control Council O. Hugo Schuck (Best Paper) Award, the 2013 Fred Ellersick Award for Best Overall MILCOM Paper, the 2011 American Society of Mechanical Engineers (ASME) Dynamics Systems and Control Division Outstanding Young Investigator Award, the 2006 IEEE Robotics and Automation Society Early Academic Career Award, an NSF CAREER Award (2006–2011), the 2004 Department of Energy Outstanding Mentor Award, and the 2001 ORNL Early Career Award for Engineering Achievement.